

SolidGen: An Autoregressive Model for Direct B-rep Synthesis

PRADEEP KUMAR JAYARAMAN, Autodesk Research, Canada
 JOSEPH G. LAMBOURNE, Autodesk Research, United Kingdom
 NISHKRIT DESAI*, University of Toronto & Vector Institute, Canada
 KARL D.D. WILLIS, Autodesk Research, USA
 ADITYA SANGHI, Autodesk Research, Canada
 NIGEL J.W. MORRIS, Autodesk Research, Canada

The Boundary representation (B-rep) format is the de-facto shape representation in computer-aided design (CAD) to model watertight solid objects. Recent approaches to generating CAD models have focused on learning sketch-and-extrude modeling sequences that are executed by a solid modeling kernel in postprocess to recover a B-rep. In this paper we present a new approach that enables learning from and synthesizing B-reps without the need for supervision through CAD modeling sequence data. Our method SolidGen, is an autoregressive neural network that models the B-rep directly by predicting the vertices, edges and faces using Transformer-based and pointer neural networks. Key to achieving this is our Indexed Boundary Representation that references B-rep vertices, edges and faces in a well-defined hierarchy to capture the geometric and topological relations suitable for use with machine learning. SolidGen can be easily conditioned on contexts e.g., class labels thanks to its probabilistic modeling of the B-rep distribution. We demonstrate qualitatively, quantitatively and through perceptual evaluation by human subjects that SolidGen can produce high quality, realistic looking CAD models.

Additional Key Words and Phrases: boundary representation, solid model, neural network, autoregressive, generative model

1 INTRODUCTION

Almost every manufactured object in the world starts life as a computer-aided design (CAD) model. The Boundary representation format (B-rep) is the de-facto standard used in CAD to represent solid objects as a watertight collection of trimmed parametric surfaces connected with well-structured topology [40]. The ability to generate B-reps automatically, driven by some context, is an enabling technology for design exploration and is critical to solving a range of problems in CAD such as reverse engineering from noisy 3D scan data, inpainting holes in solid models plausibly, and design synthesis from images or drawings.

Recent approaches to the generation of CAD models have focused on generating sequences of CAD modeling operations [43, 44, 46], rather than the underlying 3D geometry in the B-rep format. These methods produce a sequence of sketch and extrude modeling operations using a neural network and the B-rep is recovered in post-process with a solid modeling kernel that executes the operations. Although this approach generates an editable CAD model, it is currently limited to the sketch and extrude modeling operations and

*Nishkrit Desai’s work was carried out as part of an internship at Autodesk Research, Canada.

Authors’ addresses: Pradeep Kumar Jayaraman, pradeep.kumar.jayaraman@autodesk.com, Autodesk Research, Canada; Joseph G. Lambourne, joseph.lambourne@autodesk.com, Autodesk Research, United Kingdom; Nishkrit Desai, nishkrit.desai@mail.utoronto.ca, University of Toronto & Vector Institute, Canada; Karl D.D. Willis, karl.willis@autodesk.com, Autodesk Research, USA; Aditya Sanghi, aditya.sanghi@autodesk.com, Autodesk Research, Canada; Nigel J.W. Morris, nigel.morris@autodesk.com, Autodesk Research, Canada.

cannot be easily extended to support other operations. In particular, fillets and chamfers, which are widely used in CAD for structural performance and ease of manufacture, are challenging as they operate on B-rep edges which are not available until the predicted solid has been built. Furthermore, sketch-and-extrude workflows operate with 2D planar curves, hence extensions to freeform modeling are not trivial.

There are several advantages to pursuing an approach that directly synthesizes the B-rep. Firstly, significantly more CAD data exists without a stored sequence of CAD modeling operations. Files created via direct modeling or exported to common B-rep file formats do not retain a history of CAD modeling operations. In the public domain, CAD model datasets with CAD modeling operations [43, 44] are significantly smaller than those without [16]. Secondly, support for freeform curves and surfaces like Bézier and non-uniform rational B-splines, or advanced topological structures like T-splines or Catmull-Clark subdivision meshes can be provided with the ability to generate B-reps directly, as they share geometric and topological similarities. Finally, there are several problems in CAD that can only be solved with a direct B-rep synthesis approach. Examples include hole-filling for repairing solids which have poorly trimmed or missing faces due to data exchange [2, 7], patching up geometry in regions of a model where error-prone operations, such as offsetting, fail [5] and the creation of parting surfaces and shut-outs in molding workflows [4, 30]. Although heuristic algorithms exist for such applications, a learning-based method has the potential to incorporate external context (hints from users in the form of a rough sketch for example) and respect aesthetic aspects of the CAD model.

In this paper we introduce SolidGen, a generative model that directly synthesizes CAD models in the B-rep format. We make the following contributions:

- We propose SolidGen, a novel learning-based method for the direct synthesis of B-rep CAD models without the need for supervision from a sequence of CAD modeling operations.
- We propose a new representation, the indexed boundary representation, that can represent B-reps as numeric arrays suitable for use with machine learning, while still allowing the original B-rep to be completely recovered.
- We show the quantitative and qualitative performance of SolidGen in both unconditioned and class-conditioned settings, including results of a perceptual study showing SolidGen produces more realistic results than the current state-of-the-art approach.

2 RELATED WORK

Solid models are a critical part of design and engineering, with the B-rep format [18, 33, 40] used in all mechanical CAD software. Since the proliferation of the B-rep format in the 1980s, a number of research areas have been explored.

Learning from B-reps. The ability to represent B-rep data as a graph [1] has inspired recent approaches using graph neural networks for classification and segmentation problems [8, 13]. B-rep topology can also be used for custom convolutions [17] or hierarchical graph structures [14]. Rather than an *encoder*, our work focuses on a *decoder* to synthesize B-rep data directly.

Constructive Solid Geometry (CSG). In CSG, 3D shapes are formed by combining parametric primitives (e.g. cuboids, spheres) with Boolean operations (e.g. union, subtraction) into a CSG tree. By parsing the tree with an appropriate geometry kernel, a B-rep shape can be obtained. CSG approaches have been used to reconstruct ‘shape programs’ in combination with techniques from the program synthesis literature, both with [10, 15, 31, 35] and without [9, 23, 24] neural guidance. By contrast, our work applies to multiple tasks beyond reconstruction.

Sequential CAD Generation. Another line of research leverages the supervision available from modeling operations stored in parametric CAD files to directly predict sequences of CAD modeling operations. The result is editable CAD files in the form of 2D engineering sketches [11, 26, 29, 42] or 3D CAD models generated from a B-rep [43, 46] or point cloud [36] target, interactive system [19], or generative model [44]. Although sequential CAD generation approaches have made significant progress, an outstanding challenge is to extend these techniques to other modeling operations beyond sketch and extrude. Common modeling operations, such as fillet and chamfer, are challenging as they operate on B-rep edges which are not part of the representation available to the network, but rather generated as a post-process. An alternate approach might use reinforcement learning with a CAD kernel integrated into the environment, similar to [21], at the expense of extended training times due to the sparse reward space and slow CAD kernel execution times. Instead, we focus our efforts on direct synthesis of the B-rep data structure which cannot be achieved by predicting sequence of CAD modeling operations.

Direct B-rep Generation. Direct B-rep generation involves the synthesis of the underlying parametric curves/surfaces and the topology that connects them to form a solid model. Several learning-based approaches have made progress with the generation of parametric curves [39] and surfaces [32]. Yet to be addressed is the creation of topology that joins parametric curves and surfaces together to form solid models, rather than relying on pre-defined topological templates [34]. PolyGen [25] is a promising approach to joint geometry and topology synthesis where sequences of n -gon mesh vertices and faces are predicted using Transformers [37]. A key insight of this work is the use of pointer networks [38] to reference previously predicted primitives and form the underlying shape topology. Our work draws inspiration from the use of pointer networks to tackle the significantly more challenging task of direct B-rep generation.

3 REPRESENTATION

3.1 Boundary Representation

The B-rep data structure comprises several topological entities—faces, wires, edges, and vertices, depicted in Figure 1, left. *Faces* are trimmed parametric surfaces delimited by one or more *wires*. *Wires* are composed of *edges* that represent the visible interval of parametric curves. Each wire is oriented so the visible part of the surface is to the left of the directed edges in the wire. At the endpoints of the edges lie *vertices*. The B-rep data structure stores many references among entities (typically using pointers) allowing efficient constant-time querying of adjacency information [18]. The expressiveness of the B-rep data structure allows efficient implementation of solid modelling operations, but also makes it a complex representation for machine learning. In particular, the challenge arises from the existence of various topological entities that are tightly coupled with one another using pointers, and geometric entities that encompass a wide variety of parametric curves and surfaces. Although there has been significant recent progress at *encoding* B-reps [13, 17, 41], *decoding* B-reps for generation-based tasks remains an open challenge.

3.2 Indexed Boundary Representation

We now derive an indexed representation of the B-rep (Figure 1, right) that can be represented as numeric arrays suitable for use with machine learning. Importantly, this representation can be inverted back into a B-rep exactly. We currently restrict the representation to elementary curves (line and arc) and surfaces (plane, cylinder, cone, sphere and torus). We do not support B-splines and conic sections that are uncommon in mechanical CAD [16, 43]. Without loss of generality, we assume that closed faces (cylinders, cones, etc.) in the B-rep are all split on the seams. This simplifies downstream processing, for e.g., a closed cylinder with a seam is split into two four sided half-cylinders.

The indexed B-rep is analogous to the indexed list data structure used to represent polygonal meshes, e.g. the Wavefront OBJ file format [20]. The indexed list data structure can be represented numerically using two lists of numbers, and has been successfully used for generative modeling of meshes [25] and engineering sketches [42]. Just as a polygonal mesh can be represented using a topological data structure like winged edge [3], or a simple data structure like the indexed list, we show that B-reps, which are natively in the partial-entity data structure can be converted into an indexed format. However, while a polygonal mesh is restricted to straight line edges and planar faces, B-reps are more general with support for curved edges and faces, making our problem more challenging. We address this challenge by explicitly representing only the bare minimum geometric and topological information in our indexed format, and leveraging solid modeling kernels to infer the rest of the information. The indexed B-rep \mathcal{B} is comprised of three lists $\{\mathcal{V}, \mathcal{E}, \mathcal{F}\}$:

- *Vertices* \mathcal{V} contain a list of 3D point coordinates corresponding to each B-rep vertex. Additionally they contain points lying on the edges.
- *Edges* \mathcal{E} and their geometry are represented as hyperedges [42] where each hyperedge is a list of indices into \mathcal{V} . A hyperedge

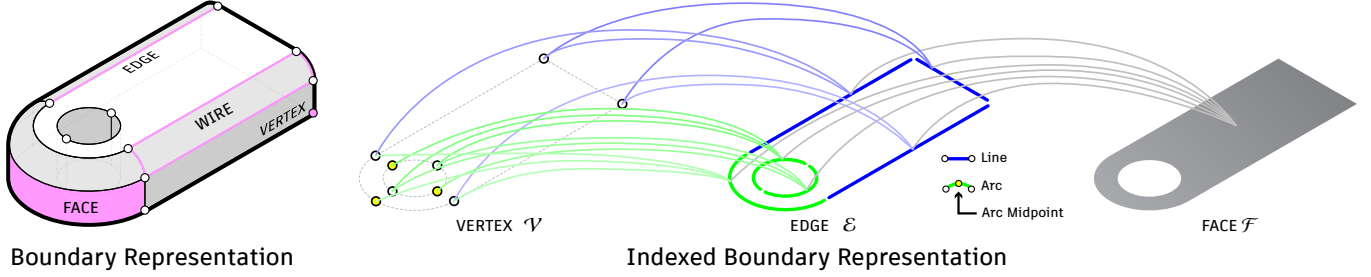


Fig. 1. The Boundary Representation (left) comprises topological entities such as faces, wires, edges, and vertices. Our Indexed Boundary Representation (right) references vertices, edges, and faces in a well-defined hierarchy suitable for use with machine learning.

connects two or more vertices to define the edge geometry. The curve type is defined by the cardinality of the hyperedge: line (2), arc (3).

- *Faces* \mathcal{F} are defined as the set of edges bounding a surface. Each face contains a list of indices pointing into \mathcal{E} .

Note that parametric surfaces that define the geometry of the face, and wires that trim the surfaces are left out of our representation and recovered in postprocess, as described next.

3.3 Recovering a Boundary Representation

The boundary curve geometry that is defined by the edges \mathcal{E} , together with the mapping of the edges that bound a face \mathcal{F} allows the wire and surface geometry to be recovered using well-defined rules. In particular, the surface type can be first fixed from the curve types while the surface parameters can be inferred from the curve and vertex geometry. For instance, faces whose vertices are coplanar define a trimmed planar surface. The surface of a face containing two arcs and two lines is likely to be a cylinder which lies along the axis defined by the lines with radius defined by the arcs. If the radii of the two arcs do not match, we can treat the surface as a trimmed cone. Faces bounded by four arcs define a torus. The only ambiguity is when a face contains a single circle on its boundary—the surface could be a plane trimmed into a disk or a hemisphere. Real world CAD data does not contain many examples like this. Spheres typically appear only on corner fillets as part of three-sided faces where the presence of three non-coplanar arcs clearly disambiguates this case. We explain the procedure in greater detail in the appendix Appendix B. Applying this rule-based procedure to every face in the indexed B-rep yields the surface type and parameters. Then, the data is read into the solid modeling kernel using the standard data exchange and shape fixing functions designed for reading neutral CAD file formats like STEP and IGES.

4 SOLIDGEN ARCHITECTURE

SolidGen is a generative model that directly synthesizes CAD models in the B-rep format. Building upon PolyGen [25] and CurveGen [42], which learn a distribution over n -gon meshes and 2D engineering sketches respectively, SolidGen enables the generation of vertices, curved edges, and non-planar faces, such that edges can refer to vertices and faces can refer to edges allowing us to build the complete B-rep topology.

Our goal is to estimate a distribution over indexed B-reps \mathcal{B} that can be sampled from to generate new indexed B-reps, and converted to actual B-reps as described in previous section. This probability distribution $p(\mathcal{B})$ is defined as the joint probability distribution of the vertices \mathcal{V} , edges \mathcal{E} , and faces \mathcal{F}

$$p(\mathcal{B}) = p(\mathcal{V}, \mathcal{E}, \mathcal{F}). \quad (1)$$

To make the learning problem tractable, we factorize this joint distribution into a product of conditionals

$$p(\mathcal{B}) = p(\mathcal{F}|\mathcal{E}, \mathcal{V})p(\mathcal{E}|\mathcal{V})p(\mathcal{V}), \quad (2)$$

and learn these distributions with separate neural networks. Once these conditional distributions are learned, B-reps can be generated by sampling vertices first, followed by edges conditioned on vertices, and faces conditioned on the edges and vertices. It is also possible to condition the generation using a context z in which case the last term in Equation 2 becomes $p(\mathcal{V}|z)p(z)$ where $p(z)$ can be derived from other representations like images, voxels, or point clouds. Since there can be an arbitrary number of vertices, edges, and faces in each B-rep, and strong symmetries are typically present in CAD models, we use autoregressive neural networks to model each of the probability distributions above. Figure 2 shows an overview of the SolidGen architecture at inference time, with each model described in further detail below.

4.1 Vertex Model

The vertex model (Figure 2, left) learns a distribution $p(\mathcal{V})$ over the vertex positions. Vertices here include both B-rep vertices and the additional points inserted on B-rep edges to encode the curve primitive information as explained in subsection 3.3. The vertices are represented as a flat sequence \mathcal{V}^{seq} by sorting \mathcal{V} lexicographically (sort by x coordinates first, y coordinates next, and z coordinates finally) into a 1D list, with a stopping token $\langle \text{EOS} \rangle$ marking the end of the vertices list. After flattening, $\mathcal{V}^{\text{seq}} = \{v_1, v_2, \dots, v_{|\mathcal{V}^{\text{seq}}|-1}, \langle \text{EOS} \rangle\}$ is of length $|\mathcal{V}^{\text{seq}}| = (|\mathcal{V}| \times 3) + 1$. The vertex model learns the following distribution

$$p(\mathcal{V}^{\text{seq}}; \theta_{\mathcal{V}}) = \prod_{t=1}^{|\mathcal{V}^{\text{seq}}|} p(v_t | v_1, v_2, \dots, v_{t-1}; \theta_{\mathcal{V}}), \quad (3)$$

where $\theta_{\mathcal{V}}$ are learnable parameters of the neural network that is a Transformer decoder [37]. The input to the Transformer decoder is derived from each of the tokens in \mathcal{V}^{seq} by learning three kinds

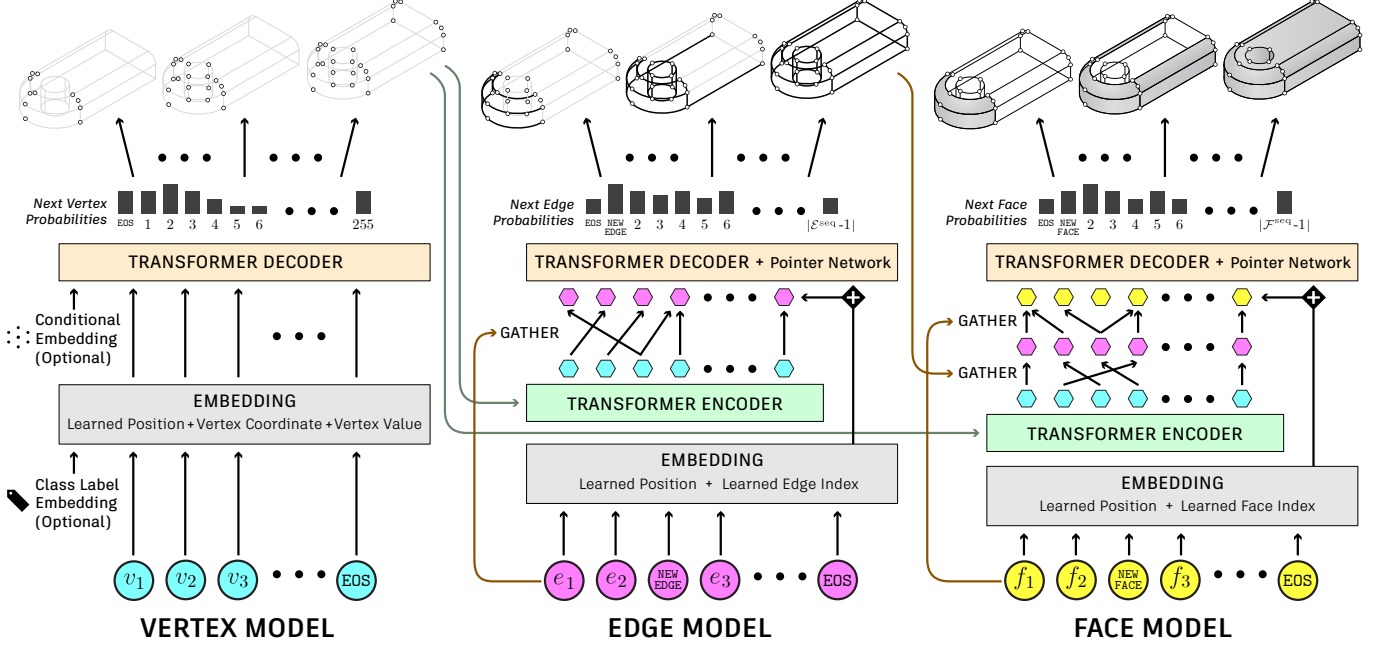


Fig. 2. The SolidGen architecture consists of a vertex (left), edge (center), and face (right) model that predict the vertices, edge connections between vertices, and face connections between edges to form an indexed B-rep (top).

of embeddings that are summed together—*coordinate embeddings* indicating whether a token is an x , y or z -coordinate, *positional embeddings* indicating the vertex index which the token belongs to, and a *value embedding* encoding the quantized x , y and z -coordinates. When class conditioning is required, a single embedding is learned from the class label and concatenated with the above embedding. At each step, the model predicts a probability distribution over all possible vertex locations for the next token. Rather than dealing with real-valued coordinates for the vertices, we quantize the vertex sequence \mathcal{V}^{seq} into 8-bits as is common in previous work [25, 29, 44]. With quantized vertices, the conditional distributions above can all be treated as categorical distributions, and the output of the network at each step is unnormalized log probabilities of dimension $2^8 + 1$ over all possible quantized positions including the $\langle \text{EOS} \rangle$ token. The model is trained with a cross-entropy loss to maximize the log-likelihood of the training data.

4.2 Edge Model

The edge model (Figure 2, center) learns a distribution $p(\mathcal{E})$ over the vertex indices. The edges are represented as a 1D list \mathcal{E}^{seq} by flattening \mathcal{E} , with a new edge token $\langle \text{NEW_EDGE} \rangle$ marking the start of a new edge and a stopping token $\langle \text{EOS} \rangle$ marking the end of the edges list. The edge sequence $\mathcal{E}^{\text{seq}} = \{e_1, e_2, \langle \text{NEW_EDGE} \rangle, \dots, e_{|\mathcal{E}^{\text{seq}}|-1}, \langle \text{EOS} \rangle\}$ is of length $|\mathcal{E}^{\text{seq}}| = \sum_{E \in \mathcal{E}} |E| + 1$, and the edge model learns the following distribution:

$$p(\mathcal{E}^{\text{seq}} | \mathcal{V}; \theta_{\mathcal{E}}) = \prod_{j=1}^{|\mathcal{E}^{\text{seq}}|} p(e_j | e_1, e_2, \dots, e_{j-1} | \mathcal{V}; \theta_{\mathcal{E}}), \quad (4)$$

where $\theta_{\mathcal{E}}$ are learnable parameters of the neural network.

Given the input vertices \mathcal{V} and current edges $\mathcal{E}_{<t}^{\text{seq}}$ until the step t , the goal is to model the next output edge token e_t as a probability distribution over the indices of \mathcal{V} . This is done by first learning *value embeddings* $\mathbf{h}_{\mathcal{V}} \in \mathbb{R}^{|\mathcal{V}| \times 256}$ from the input vertices $\mathcal{V} = \{(x_i, y_i, z_i)\}_{i=0}^{|\mathcal{V}|-1}$:

$$\mathbf{h}_{\mathcal{V}} = \{\text{Embed}_x(x_i) + \text{Embed}_y(y_i) + \text{Embed}_z(z_i)\}_{i=0}^{|\mathcal{V}|-1}, \quad (5)$$

and $\langle \text{NEW_EDGE} \rangle$ and $\langle \text{EOS} \rangle$ token embeddings $\mathbf{h}_{\langle \text{NEW_EDGE} \rangle} \in \mathbb{R}^{1 \times 256}$ and $\mathbf{h}_{\langle \text{EOS} \rangle} \in \mathbb{R}^{1 \times 256}$, respectively. These are all concatenated to form a total of $|\mathcal{V}| + 2$ input embeddings. Learned *positional embeddings* indicating the position of each token, and learned *edge index embeddings* that map each token to its corresponding edge are further summed with this input. A Transformer encoder $T_{\text{enc}}^{\mathcal{E}}$ is then used to embed this input into $\mathbf{h}_{\text{inp}} \in \mathbb{R}^{(|\mathcal{V}|+2) \times 256}$.

$$\mathbf{h}_{\text{inp}} = T_{\text{enc}}^{\mathcal{E}}(\mathbf{h}_{\langle \text{EOS} \rangle} \parallel \mathbf{h}_{\langle \text{NEW_EDGE} \rangle} \parallel \mathbf{h}_{\mathcal{V}}),$$

where \parallel is the concatenation operator. Then, edge embeddings $\mathbf{h}_{\mathcal{E}_{<t}^{\text{seq}}} \in \mathbb{R}^{|\mathcal{E}_{<t}^{\text{seq}}| \times 256}$ are formed by gathering the input embeddings \mathbf{h}_{inp} corresponding to the vertex indices in $\mathcal{E}_{<t}^{\text{seq}}$.

$$\mathbf{h}_{\mathcal{E}_{<t}^{\text{seq}}} = \{\mathbf{h}_{\text{inp}}[e_j]\}_{j=1}^{t-1}.$$

A Transformer decoder $T_{\text{dec}}^{\mathcal{E}}$ then outputs a pointer vector \mathbf{p}_t that is compared to the input embeddings \mathbf{h}_{inp} using a dot product operation and normalized using softmax to get a distribution over the $1 \leq k \leq |\mathcal{V}| + 2$ input vertex indices and $\langle \text{NEW_EDGE} \rangle, \langle \text{EOS} \rangle$ tokens:

$$\mathbf{p}_t = T_{\text{dec}}^{\mathcal{E}}(\mathbf{h}_{\mathcal{E}_{<t}^{\text{seq}}}),$$

$$p(e_t = k | \mathcal{E}_{<t}^{\text{seq}}, \mathcal{V}) = \text{softmax}_k(\mathbf{p}_t \cdot \mathbf{h}_{\text{inp}}[k]).$$

The model is trained using the cross-entropy loss to predict the distribution $p(e_t = k \mid \mathcal{E}_{<t}^{\text{seq}}, \mathcal{V})$ which is repeatedly created at each time step and sampled to generate the edge tokens autoregressively. During training, ground-truth is used for conditioning (i.e., teacher-forcing) rather than previous samples.

4.3 Face Model

The face model (Figure 2, right) learns a distribution $p(\mathcal{F})$ over the faces. The faces are represented as a flat sequence \mathcal{F}^{seq} similar to the edges by flattening \mathcal{F} into a 1D list, with a new face token $\langle \text{NEW_FACE} \rangle$ marking the start of a new face and a stopping token $\langle \text{EOS} \rangle$ marking the end of the faces list. The model learns the following probability distribution:

$$p(\mathcal{F}^{\text{seq}} \mid \mathcal{E}, \mathcal{V}; \theta_{\mathcal{F}}) = \prod_{t=1}^{|\mathcal{F}^{\text{seq}}|} p(f_t \mid f_1, f_2, \dots, f_{t-1} \mid \mathcal{E}, \mathcal{V}; \theta_{\mathcal{F}}), \quad (6)$$

where $\theta_{\mathcal{F}}$ are learnable parameters of the neural network.

The face model functions similarly as the edge model and represents the face features by gathering edge embeddings. Given the input vertices \mathcal{V} and edges \mathcal{E} , and the current faces $\mathcal{F}_{<t}^{\text{seq}}$ at step t , the goal is to model the next output face token f_t as a probability distribution over the indices of \mathcal{E} .

This is done by learning vertex embeddings $\mathbf{h}_{\mathcal{V}} \in \mathbb{R}^{|\mathcal{V}| \times 256}$ from the input vertices as in Equation 5. The rows of $\mathbf{h}_{\mathcal{V}}$ corresponding to the vertex indices in \mathcal{E} are first gathered and summed to form edge embeddings $\mathbf{h}_{\mathcal{E}}$:

$$\mathbf{h}_{\mathcal{E}} = \{\sum_{v \in E} \mathbf{h}_{\mathcal{V}}[v]\}_{E \in \mathcal{E}}.$$

Intuitively, the edge embeddings are defined based on the embeddings of their endpoint vertices. Then, face embeddings $\mathbf{h}_{\mathcal{F}_{<t}^{\text{seq}}}$ are formed by gathering the edge embeddings:

$$\mathbf{h}_{\mathcal{F}_{<t}^{\text{seq}}} = \{\mathbf{h}_{\mathcal{E}}[f_k]\}_{k=1}^{t-1}.$$

Next $\langle \text{NEW_FACE} \rangle$ and $\langle \text{EOS} \rangle$ token embeddings $\mathbf{h}_{\langle \text{NEW_FACE} \rangle}$ and $\mathbf{h}_{\langle \text{EOS} \rangle}$ are formed and these are all concatenated to form a total of $|\mathcal{E}| + 2$ input embeddings. Learned *positional embeddings* indicating the position of each token, and learned *face index embeddings* that map each token to its corresponding face are further summed with this input. A Transformer encoder $T_{\text{enc}}^{\mathcal{F}}$ is then used to embed this input into \mathbf{h}_{inp} .

$$\mathbf{h}_{\text{inp}} = T_{\text{enc}}^{\mathcal{F}}(\mathbf{h}_{\langle \text{EOS} \rangle} \parallel \mathbf{h}_{\langle \text{NEW_FACE} \rangle} \parallel \mathbf{h}_{\mathcal{E}}).$$

The idea here is to encode faces by the embeddings of the edges that lie on their boundary. A Transformer decoder $T_{\text{dec}}^{\mathcal{F}}$ then outputs a pointer vector \mathbf{p}_t that is compared to the edge embeddings $\mathbf{h}_{\mathcal{E}}$ using a dot product operation and normalized using softmax to get a distribution over the $1 \leq k \leq |\mathcal{E}| + 2$ input edge indices and $\langle \text{NEW_FACE} \rangle$, $\langle \text{EOS} \rangle$ tokens:

$$\mathbf{p}_t = T_{\text{dec}}^{\mathcal{F}}(\mathbf{h}_{\mathcal{F}_{<t}^{\text{seq}}}),$$

$$p(f_t = k \mid \mathcal{F}_{<t}^{\text{seq}}, \mathcal{E}, \mathcal{V}) = \text{softmax}_k(\mathbf{p}_t \cdot \mathbf{h}_{\mathcal{E}}[k]).$$

The face model is also trained by teacher-forcing to maximize the log-likelihood of the ground truth face sequence using a cross-entropy loss.

4.4 Masking Invalid Outputs

An indexed B-rep can be easily validated for correctness. During inference, we discard obviously invalid samples by performing certain checks, and only return valid samples. We consider the following criteria that are necessary but not sufficient to build a valid B-rep, and improve the quality of samples produced by the model.

- The length of the vertex sequence produced by the model, excluding the $\langle \text{EOS} \rangle$ token must be divisible by 3.
- The $\langle \text{NEW_EDGE} \rangle$ token must appear after every 2 (line) or 3 (arc) edge tokens.
- The edge tokens belonging to the same edge must be unique.
- Each face must be bounded by a closed set of edges.

During the autoregressive sampling, it is also possible to mask the invalid logits that do not satisfy these criteria at each time step, and distribute the next token probabilities among the valid tokens [25]. This could potentially improve sample quality further, however, we do not do this for simplicity.

5 EXPERIMENTS

In this section we perform experiments to qualitatively and quantitatively evaluate the unconditioned generation and class-conditional generation tasks. We begin by detailing the implementation and experiment setup.

5.1 Implementation Details

Our implementation is in PyTorch. We find it critical for convergence to use the pre-LayerNorm variant of the Transformer [45]. We train our models with the Adam optimizer initialized with learning rate 10^{-4} . We use gradient clipping (at magnitude 1.0) and stochastic weight averaging for improved training stability and generalization. The vertex, edge, and face models can be trained in parallel since we employ teacher-forcing where the models are decoupled during training—rather than using the samples from one model to condition to subsequent model, we use the ground truth data. To sample from the models we use nucleus/top-p sampling [12] with a top-p value of 0.9. Before sampling we modulate the logits by a temperature $\tau = 0.8$ for the vertex model and 0.75τ and 0.65τ for the edge and face models, respectively. We use the solid modeling kernel OpenCascade/pythonOCC [27] for all data processing.

5.2 Datasets

Publicly available datasets for B-rep solid models are limited compared to other 3D representations. We demonstrate our method on two datasets. Note that in all datasets, we only consider files that contain the surface and curve types supported by the indexed B-rep format.

The Parametric Variations (PVar) Dataset is synthetically designed for testing SolidGen on the class-conditional generation task, since categorically labeled B-rep datasets are unavailable. It consists of 60 template solids with parameters controlling both the sketch dimensions, extrusion distances and wires that are extruded. By varying these parameters we can generate solids with different geometries but near-identical topology. A total of 120,000 models, 2000 for each of the 60 topological templates were created. The solids generated from each distinct template are considered to belong to the same

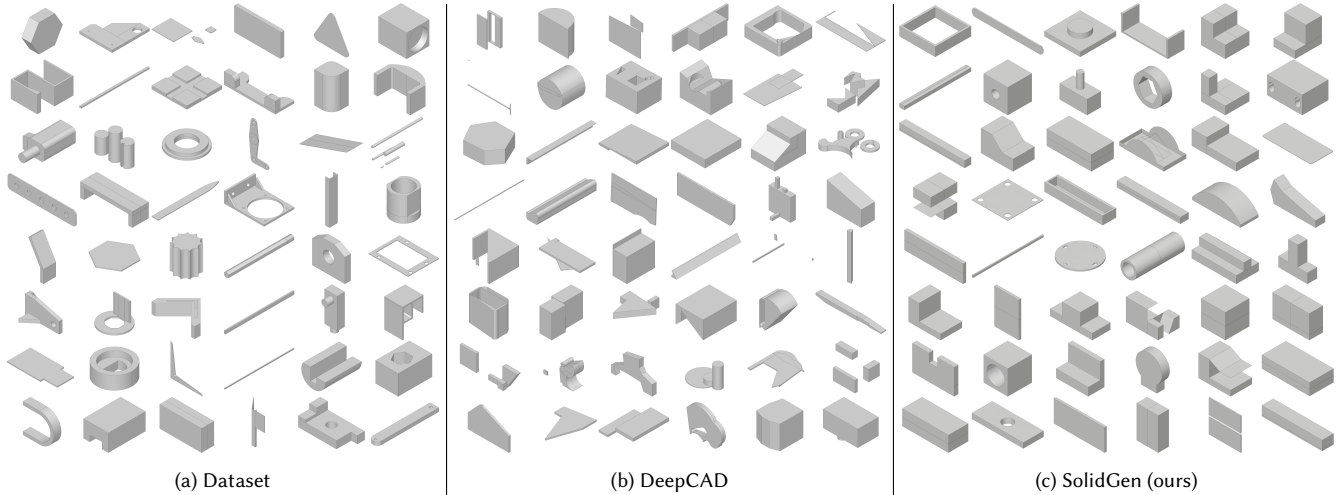


Fig. 3. Qualitative results for unconditional generation. Samples from the DeepCAD dataset (a), generated by SolidGen (b), and generated by DeepCAD (c).

class. The dataset is split in a 90 (train)/5 (validation)/5 (test) proportion.

The *DeepCAD Dataset* [44] contains a subset of the CAD models available in the ABC dataset [16] that additionally includes the sequence of sketch and extrude CAD modeling operations. The original dataset contains 178,238 CAD models, however, we find a significant portion of duplicate models are present. We use a hash-based method, described in Appendix A of the supplementary material, to remove duplicates. We filter out trivial (< 8 faces) and overly-complex (> 130 faces) models. This yields 64,449 train, 3,578 validation and 3,577 test data.

5.3 Metrics

We use the following metrics to quantitatively evaluate and compare SolidGen with other methods. Valid, novel and unique metrics are computed based on our hashing procedure described in Appendix A of the supplementary material.

Valid The percentage of valid B-reps is reported and considers three factors: (1) every face in the B-rep must generate at least one triangle. If not, the B-rep is considered invalid as it cannot be rendered properly and is not possible to manufacture. (2) The edges in each wire in the B-rep must be ordered correctly. (3) The wires should not self-intersect. This ensures that faces are well-defined and surfaces trimmed correctly.

Novel The percentage of valid B-reps in the sample set that are not available in the training set captures the novelty of the generated samples. A lower number implies that the model is memorizing the training set.

Unique The percentage of distinct valid B-reps generated within the sample set is reported and captures the diversity of the samples generated by the model. A lower value indicates the model is limited in producing design variations.

Accuracy For class-conditional generation, we report the percentage of B-reps in the sample set that come from the desired input class. We compute this by comparing the topology-only hash for

Table 1. Quality of 1000 random unconditional samples generated by networks trained on the DeepCAD [44] dataset. All numbers are percentages.

Method	Valid (\uparrow)	Novel (\uparrow)	Unique (\uparrow)
Ours	92.133	86.638	89.146
DeepCAD	72.067	99.214	99.861

each generated solid against the hashes of the solids in the training set belonging to the input category. A low accuracy means that the model is unable to incorporate class-conditioning.

5.4 Unconditional Generation

5.4.1 Comparison with DeepCAD. In this section we compare the unconditional modeling performance of SolidGen with that of DeepCAD [44]. While SolidGen is a generative model that directly synthesizes B-reps, DeepCAD is an autoencoder that employs a GAN to generate sequences of sketch and extrude operations. Although both models work in fundamentally different ways, we strive to provide a one-to-one comparison by limiting the training data for SolidGen to the narrower scope required by DeepCAD. Specifically, we train SolidGen on the B-reps obtained from the DeepCAD dataset [44], while DeepCAD uses additional supervision from sequences of CAD modeling operations.

Figure 3 shows qualitative results for unconditional generation trained on the DeepCAD dataset [44]. We show samples from the dataset for comparison (a), along with generated samples from DeepCAD (b) and SolidGen (c). We also evaluate the models quantitatively in Table 1 using the metrics described in subsection 5.3. We find that SolidGen produces B-reps that are more representative of the training set. A large portion of the models produced by SolidGen (92.1%) are valid and usable B-reps compared to DeepCAD (72.1%). We attribute this to the three main factors: (1) The indexed B-rep is more representative of the final B-rep compared to sketch-and-extrude sequences, hence a correct indexed B-rep output is likely to

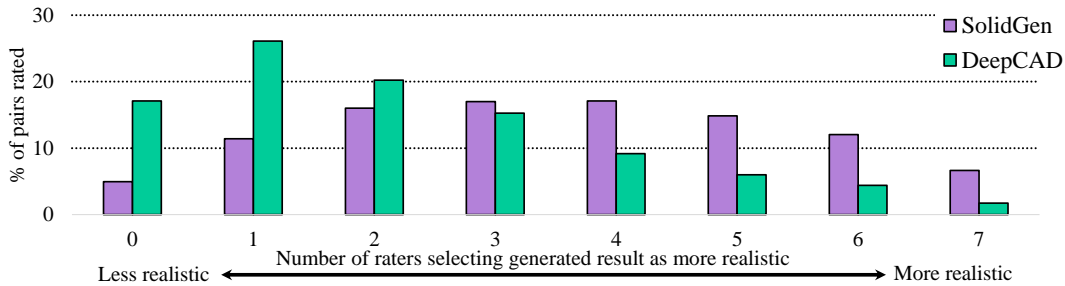


Fig. 4. Human perceptual study showing the distribution of votes by 7 human evaluators for the realism of SolidGen and DeepCAD models compared to samples from the training set.

be convertible into a valid B-rep. (2) The indexed B-rep output of the network can be easily verified for correctness based on the masking procedure described in subsection 4.4. (3) The learning problem is simplified when the challenging task of generating B-reps is factorized into smaller sub-problems of generating vertices, edges and faces. Among the valid sample set, SolidGen produces less unique and novel B-reps (86.7% and 89.2%) than DeepCAD (99.2% and 99.9%). We observe that many of DeepCAD’s valid samples are noisy and unrealistic which artificially increases the unique and novel scores. We further investigate this through a human perceptual study next.

Human Perceptual Evaluation. Rather than rely only on quantitative metrics, we believe it is critical to perform human evaluation on the output of generative models. To evaluate the realism of the generated samples, we perform a perceptual study using human evaluators recruited through Amazon’s Mechanical Turk service [22]. The crowd workers were shown pairs of images, one of which was generated by SolidGen or DeepCAD and the other randomly selected from the training set, and asked to judge which of the two was more realistic. Each image pair was rated by 7 different human evaluators and we record the number of workers who selected the generated model as more realistic. The results are shown in Figure 4. We see that for SolidGen the distribution is roughly symmetric with the majority vote judging the SolidGen output to be more realistic 50.6% of the time. This indicates the realism of the SolidGen output is indistinguishable from the training set. For DeepCAD we see the distribution is skewed to the left, with the majority vote judging the DeepCAD output to be more realistic only 21.3% of the time.

5.5 Class-conditional Generation

SolidGen can be trained conditionally based on a wide range of contexts. Here, we demonstrate that class labels in the PVar dataset can be used for conditioning and evaluate the quality and accuracy of the samples produced by the model. The class conditional model uses the same architecture and hyperparameters as the unconditional model. The class label embedding is obtained by learning a 256-dimensional embedding from the input class label. This class embedding is concatenated with the vertex model’s coordinate, position and value embeddings (see Figure 2) and serves as a global context that will be utilized by the Transformer decoder. The edge

Table 2. Quality of class-conditional samples generated by SolidGen trained on our PVar dataset. All numbers are percentages.

Valid (↑)	Novel (↑)	Unique (↑)	Accuracy (↑)
99.167	90.294	98.655	75.198

and face model remain unchanged. Qualitative results of our class-conditioning model given random class labels as input are shown in Figure 5 where it is clear that the model is able to leverage the hint given by the class label to generate samples similar to data in the training set, with variations in geometry and topology. Quantitative evaluation of the generated samples (40 per-class totalling to 2400 samples) are provided in Table 2. We see that SolidGen generates a high number of valid B-reps (99.2%), with 98.7% being unique in the sample set demonstrating diversity, and 90.3% being novel compared to the training set. 75.2% of the samples pertain to the desired input category based on our accuracy metric that considers topological matches. Note that slight changes in topology can misclassify the samples; visually we find all samples to be drawn from the same class.

6 DISCUSSION & CONCLUSION

Limitations. Our current method has some limitations that can be addressed in future work. Extremely complex CAD models with long sequence lengths increase the training time and chance for compounding errors at test time, which could be attributed to teacher forcing. Our indexed B-rep format currently supports the most common types of curves and surfaces found in mechanical CAD models but not conic sections and splines that are common in freeform modeling. Conics, e.g. ellipses, can be supported in a similar way to circular arcs, to expand the range of CAD models our method can consume. A straightforward extension to support B-splines is to convert them into cubic Bézier curves by knot insertion and define a new edge type that groups four vertices. Like previous generative neural networks [25, 42, 44] our method is trained using classification losses. Several important CAD applications, e.g., reverse engineering, require reconstruction losses that incorporate the B-rep geometry. Differentiable sampling and reinforcement learning are promising approaches to explore this direction.

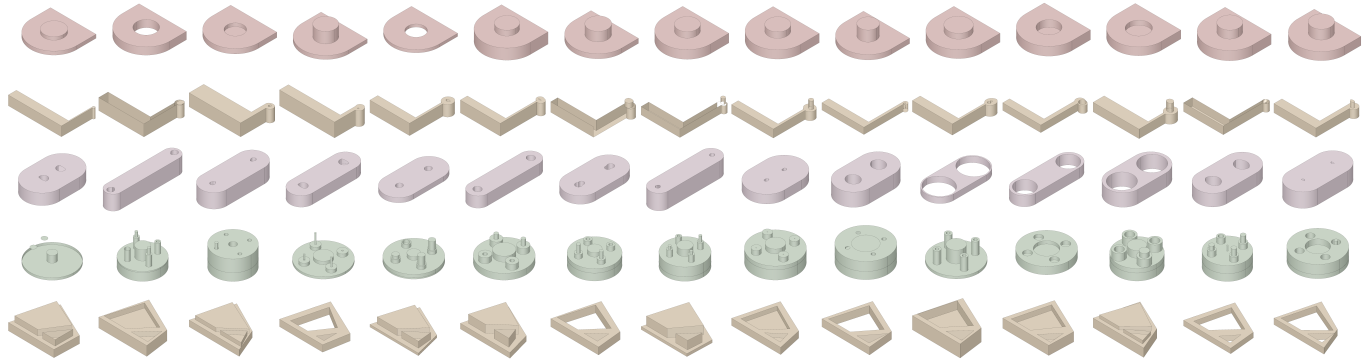


Fig. 5. Class-conditional generation by SolidGen trained on the PVar dataset. Each row shows samples generated from the same class.

Conclusion. We presented SolidGen, a generative model that can directly learn from and synthesize boundary representation (B-rep) CAD models without the need for supervision from a sequence of CAD modeling operations. We achieved this by deriving the indexed B-rep format that captures the hierarchical nature of B-rep vertices, edges and faces in a new machine learning friendly representation. SolidGen generates highly coherent yet diverse B-reps of arbitrary complexity as demonstrated in our comparison with prior work. As our method can generate local regions of B-rep topology in addition to entire solids, this allows learning based techniques to play a role in many other workflows such as solid model inpainting and parting surface creation.

REFERENCES

- [1] Silvia Ansaldo, Leila De Floriani, and Bianca Falcidieno. 1985. Geometric modeling of solid objects by using a face adjacency graph representation. *Annual Conference on Computer Graphics and Interactive Techniques (SIGGRAPH)* 19, 3 (1985), 131–139.
- [2] Armand Daryoush Assadi. 2003. *CAD model robustness assessment and repair*. Ph. D. Dissertation. Iowa State University, Ames, Iowa.
- [3] Bruce G. Baumgart. 1972. *Winged Edge Polyhedron Representation*. Technical Report. Stanford University, Stanford, CA, USA.
- [4] Rahul Bhargava, Lee Elliot Weiss, Friedrich B Prinz, et al. 1991. *Automated ejectability analysis and parting surface generation for mold tool design*. [Carnegie Mellon University], Engineering Design Research Center.
- [5] Garrett Bodily. 2014. *A Computational Hybrid Method for Self-Intersection Free Offsetting of CAD Geometry*. Brigham Young University.
- [6] William Bouma, Ioannis Fudos, Christoph Hoffmann, Jiazhen Cai, and Robert Paige. 1995. Geometric constraint solver. *Computer-Aided Design* 27, 6 (1995), 487–501. [https://doi.org/10.1016/0010-4485\(94\)00013-4](https://doi.org/10.1016/0010-4485(94)00013-4)
- [7] Geoffrey Butlin and Clive Stops. 1996. CAD data repair. In *Proceedings of the 5th International Meshing Roundtable*. Citeseer, 7–12.
- [8] Weijuan Cao, Trevor Robinson, Yang Hua, Flavien Bousuge, Andrew R. Colligan, and Wanbin Pan. 2020. Graph Representation of 3D CAD Models for Machining Feature Recognition With Deep Learning. In *Proceedings of the ASME 2020 International Design Engineering Technical Conferences and Computers and Information in Engineering Conference (IDETC-CIE)*. ASME.
- [9] Tao Du, Jeevana Priya Inala, Yewen Pu, Andrew Spielberg, Adriana Schulz, Daniela Rus, Armando Solar-Lezama, and Wojciech Matusik. 2018. Inversecsg: Automatic conversion of 3d models to csg trees. *Annual Conference on Computer Graphics and Interactive Techniques (SIGGRAPH)* 37, 6 (2018), 1–16.
- [10] Kevin Ellis, Maxwell Nye, Yewen Pu, Felix Sosa, Josh Tenenbaum, and Armando Solar-Lezama. 2019. Write, execute, assess: Program synthesis with a repl. In *Advances in Neural Information Processing Systems (NeurIPS)*. 9169–9178.
- [11] Yaroslav Ganin, Sergey Bartunov, Yujia Li, Ethan Keller, and Stefano Saliceti. 2021. Computer-aided design as language. In *Advances in Neural Information Processing Systems (NeurIPS)*.
- [12] Ari Holtzman, Jan Buys, Li Du, Maxwell Forbes, and Yejin Choi. 2020. The Curious Case of Neural Text Degeneration. In *8th International Conference on Learning Representations, ICLR*. OpenReview.net. <https://openreview.net/forum?id=rygGQyrFvH>
- [13] Pradeep Kumar Jayaraman, Aditya Sanghi, Joseph G. Lambourne, Karl D.D. Willis, Thomas Davies, Hooman Shayani, and Nigel Morris. 2021. UV-Net: Learning From Boundary Representations. In *IEEE Conference on Computer Vision and Pattern Recognition (CVPR)*. 11703–11712.
- [14] Benjamin Jones, Dalton Hildreth, Duowen Chen, Ilya Baran, Vladimir G Kim, and Adriana Schulz. 2021. AutoMate: a dataset and learning approach for automatic mating of CAD assemblies. *Annual Conference on Computer Graphics and Interactive Techniques Asia (SIGGRAPH Asia)* 40, 6 (2021), 1–18.
- [15] Kacper Kania, Maciej Zięba, and Tomasz Kajdanowicz. 2020. UCSG-Net—Unsupervised Discovering of Constructive Solid Geometry Tree. In *Advances in Neural Information Processing Systems (NeurIPS)*.
- [16] Sebastian Koch, Albert Matveev, Zhongshi Jiang, Francis Williams, Alexey Artemov, Evgeny Burnaev, Marc Alexa, Denis Zorin, and Daniele Panofzo. 2019. ABC: A Big CAD Model Dataset For Geometric Deep Learning. In *The IEEE Conference on Computer Vision and Pattern Recognition (CVPR)*. 12773–12782.
- [17] Joseph G. Lambourne, Karl D.D. Willis, Pradeep Kumar Jayaraman, Aditya Sanghi, Peter Meltzer, and Hooman Shayani. 2021. BRPNet: A Topological Message Passing System for Solid Models. In *IEEE Conference on Computer Vision and Pattern Recognition (CVPR)*. 12773–12782.
- [18] Sang Hun Lee and Kunwoo Lee. 2001. Partial Entity Structure: A Compact Non-Manifold Boundary Representation Based on Partial Topological Entities. In *Proceedings of the Sixth ACM Symposium on Solid Modeling and Applications (SMA '01)*. Association for Computing Machinery, New York, NY, USA, 159–170. <https://doi.org/10.1145/376957.376976>
- [19] Changjian Li, Hao Pan, Adrien Bousseau, and Niloy J Mitra. 2020. Sketch2cad: Sequential cad modeling by sketching in context. *ACM Transactions on Graphics (TOG)* 39, 6 (2020), 1–14.
- [20] Sustainability of Digital Formats Library of Congress. 2020. *Wavefront OBJ File Format*. <https://www.loc.gov/preservation/digital/formats/fdd/fdd000507.shtml>
- [21] Cheng Lin, Tingxiang Fan, Wenping Wang, and Matthias Nießner. 2020. Modeling 3D Shapes by Reinforcement Learning. In *European Conference on Computer Vision (ECCV)*.
- [22] Abhishek Mishra. 2019. Machine Learning in the AWS Cloud: Add Intelligence to Applications with Amazon SageMaker and Amazon Rekognition. <https://aws.amazon.com/sagemaker/groundtruth/>
- [23] Chandrakana Nandi, Anat Caspi, Dan Grossman, and Zachary Tatlock. 2017. Programming language tools and techniques for 3D printing. In *2nd Summit on Advances in Programming Languages (SNAPL 2017)*. Schloss Dagstuhl-Leibniz-Zentrum fuer Informatik.
- [24] Chandrakana Nandi, James R Wilcox, Pavel Panchekha, Taylor Blau, Dan Grossman, and Zachary Tatlock. 2018. Functional programming for compiling and decompiling computer-aided design. *Proceedings of the ACM on Programming Languages* 2, ICFP (2018), 1–31.
- [25] Charlie Nash, Yaroslav Ganin, SM Ali Eslami, and Peter Battaglia. 2020. Polygen: An autoregressive generative model of 3d meshes. In *International Conference on Machine Learning (ICML)*. PMLR, 7220–7229.
- [26] Wamiq Reyaz Para, Shariq Farooq Bhat, Paul Guerrero, Tom Kelly, Niloy Mitra, Leonidas Guibas, and Peter Wonka. 2021. SketchGen: Generating Constrained CAD Sketches. In *Advances in Neural Information Processing Systems (NeurIPS)*.
- [27] Thomas Paviot. [n. d.]. pythonOCC, 3D CAD/CAE/PLM development framework for the Python programming language. <https://dev.opencascade.org/project/pythonocc> (Accessed 05-Mar-2022).
- [28] Ari Seff, Yaniv Ovadia, Wenda Zhou, and Ryan P. Adams. 2020. SketchGraphs: A Large-Scale Dataset for Modeling Relational Geometry in Computer-Aided

- Design. In *ICML 2020 Workshop on Object-Oriented Learning*.
- [29] Ari Seff, Wenda Zhou, Nick Richardson, and Ryan P Adams. 2021. Vitruvion: A Generative Model of Parametric CAD Sketches. *arXiv:2109.14124* (2021).
- [30] Mouhsine Serrar and Gary A. Gabriele. 1995. Automatic Generation of Parting Surfaces and Mold Halves. In *ASME 1995 15th International Computers in Engineering Conference and the ASME 1995 9th Annual Engineering Database Symposium (International Design Engineering Technical Conferences and Computers and Information in Engineering Conference)*. 75–82.
- [31] Gopal Sharma, Rishabh Goyal, Difan Liu, Evangelos Kalogerakis, and Subhransu Maji. 2018. CSGNet: Neural Shape Parser for Constructive Solid Geometry. In *IEEE Conference on Computer Vision and Pattern Recognition (CVPR)*.
- [32] Gopal Sharma, Difan Liu, Subhransu Maji, Evangelos Kalogerakis, Siddhartha Chaudhuri, and Radomir Měch. 2020. Parsenet: A parametric surface fitting network for 3d point clouds. In *European Conference on Computer Vision (ECCV)*. Springer, 261–276.
- [33] Sergey Slyadnev, Alexander Malyshev, Andrey Voevodin, and Vadim Turlapov. 2020. On the Role of Graph Theory Apparatus in a CAD Modeling Kernel. *Proceedings of GraphiCon 2020* (2020).
- [34] Dmitriy Smirnov, Mikhail Bessmeltsev, and Justin Solomon. 2021. Learning Manifold Patch-Based Representations of Man-Made Shapes. In *International Conference on Learning Representations (ICLR)*.
- [35] Yonglong Tian, Andrew Luo, Xingyuan Sun, Kevin Ellis, William T. Freeman, Joshua B. Tenenbaum, and Jiajun Wu. 2019. Learning to Infer and Execute 3D Shape Programs. In *International Conference on Learning Representations (ICLR)*.
- [36] Mikaela Angelina Uy, Yen-yu Chang, Minhyuk Sung, Purvi Goel, Joseph Lambourne, Tolga Birdal, and Leonidas J. Guibas. 2021. Point2Cyl: Reverse Engineering 3D Objects from Point Clouds to Extrusion Cylinders. *CoRR abs/2112.09329* (2021). [arXiv:2112.09329](https://arxiv.org/abs/2112.09329) <https://arxiv.org/abs/2112.09329>
- [37] Ashish Vaswani, Noam Shazeer, Niki Parmar, Jakob Uszkoreit, Llion Jones, Aidan N. Gomez, Lukasz Kaiser, and Illia Polosukhin. 2017. Attention is All You Need. In *Proceedings of the 31st International Conference on Neural Information Processing Systems (Long Beach, California, USA) (NIPS'17)*. Curran Associates Inc., Red Hook, NY, USA, 6000–6010.
- [38] Oriol Vinyals, Meire Fortunato, and Navdeep Jaitly. 2015. Pointer networks. *Advances in Neural Information Processing Systems (NeurIPS)* (2015).
- [39] Xiaogang Wang, Yuelang Xu, Kai Xu, Andrea Tagliasacchi, Bin Zhou, Ali Mahdavi-Amiri, and Hao Zhang. 2020. PIE-NET: Parametric Inference of Point Cloud Edges. In *Advances in Neural Information Processing Systems*, Vol. 33. Curran Associates, Inc., 20167–20178.
- [40] K.J. Weiler. 1986. *Topological structures for geometric modeling*. University Microfilms.
- [41] Karl DD Willis, Pradeep Kumar Jayaraman, Hang Chu, Yunsheng Tian, Yifei Li, Daniele Grandi, Aditya Sanghi, Linh Tran, Joseph G Lambourne, Armando Solar-Lezama, et al. 2021. JoinABLE: Learning Bottom-up Assembly of Parametric CAD Joints. *arXiv:2111.12772* (2021).
- [42] Karl DD Willis, Pradeep Kumar Jayaraman, Joseph G Lambourne, Hang Chu, and Yewen Pu. 2021. Engineering sketch generation for computer-aided design. In *IEEE Conference on Computer Vision and Pattern Recognition Workshops (CVPR Workshop)*. 2105–2114.
- [43] Karl D. D. Willis, Yewen Pu, Jieliang Luo, Hang Chu, Tao Du, Joseph G. Lambourne, Armando Solar-Lezama, and Wojciech Matusik. 2021. Fusion 360 Gallery: A Dataset and Environment for Programmatic CAD Construction from Human Design Sequences. *ACM Transactions on Graphics (TOG)* 40, 4 (2021).
- [44] Rundi Wu, Chang Xiao, and Changxi Zheng. 2021. DeepCAD: A Deep Generative Network for Computer-Aided Design Models. In *IEEE International Conference on Computer Vision (ICCV)*. 6772–6782.
- [45] Ruibin Xiong, Yunchang Yang, Di He, Kai Zheng, Shuxin Zheng, Chen Xing, Huishuai Zhang, Yanyan Lan, Liwei Wang, and Tieyan Liu. 2020. On Layer Normalization in the Transformer Architecture. In *Proceedings of the 37th International Conference on Machine Learning (Proceedings of Machine Learning Research, Vol. 119)*, Hal Daumé III and Aarti Singh (Eds.). PMLR, 10524–10533. <https://proceedings.mlr.press/v119/xiong20b.html>
- [46] Xianghao Xu, Wenzhe Peng, Chin-Yi Cheng, Karl D.D. Willis, and Daniel Ritchie. 2021. Inferring CAD Modeling Sequences Using Zone Graphs. In *IEEE Conference on Computer Vision and Pattern Recognition (CVPR)*. 6062–6070.

APPENDIX

A HASHING INDEXED B-REPS

We use duplication detection [42] tools to compare B-reps. This is used, for example, to assess the degree to which the generated B-reps exactly match with those in the training set, quantify the diversity of samples generated by SolidGen, etc. The duplicate detection algorithm is based on the Weisfeiler Lehman isomorphism test. Two graphs are built from the B-rep—a face adjacency graph [1] where the B-rep faces are graph nodes and adjacent faces are connected by graph edges, and a vertex adjacency graph where B-rep vertices are graph nodes and the B-rep edges are graph edges. The quantized vertex positions are used to initialize the vertex hashes and stored as node attributes, and the curve type information is stored as edge attributes, making the final hash dependent on the solid geometry. The final hash string for each solid is created by concatenating the graph hashes of the face adjacency and vertex adjacency graphs. Hashes can be topology-only (in which case the curve and vertex geometry are not populated as graph attributes) or consider both geometry and topology.

B CONVERTING INDEXED B-REPS TO B-REPS

Here we detail the complete method to convert indexed B-reps to B-reps.

Vertices and Edges. Each point in \mathcal{V} is potentially a B-rep vertex. Each edge $E \in \mathcal{E}$ is used to dereference into \mathcal{V} and collect the list of points defining the edge and its geometry. The endpoints of E are used to construct a pair of B-rep vertices if they do not already exist, and the topological B-rep edge connecting them. The curve geometry is defined by the cardinality of E : two points define a line, while three points define an arc (see Figure 1 right).

Wires. Next, we examine each face in \mathcal{F} to gather the list of edges bounding it. Note that edges bounding a face can either be part of an outer wire running in counter-clockwise direction that defines the visible part of the face’s geometry, or part of one or more inner wires running in clockwise direction that define the hidden portion (holes) in the face’s geometry. Our goal here is to form these wires by connecting the given set of edges into one or more closed loops. We achieve this by defining a vertex-edge graph where each B-rep edge and its vertices are graph nodes connected by directed edges and detecting cycles in this graph (see Figure A1 (a)). Each cycle (except trivial ones) defines a wire, and the outer wire is defined as the largest wire (based on the extents of its bounding box). The other wires are assumed to run in clockwise direction and define holes.

Surfaces. We support five prismatic parametric surface types that are common in CAD: plane, cylinder, cone, sphere, and torus. We develop an algorithm that identifies the surface type by finding the simplest surface consistent with the boundary curves in the wires bounding a face within a prescribed tolerance (see Figure A1 (b)).

If all curves in the wire are coplanar then a plane is fitted. Otherwise, the curves are checked for consistency with a cylinder, cone, sphere and torus in that order.

If a wire has two arcs and two lines, then a cylinder can be defined by the radius and axis of each arc in the wire. Furthermore, we can check if the axis of cylinders are coaxial and parallel to the lines in the wire. If the radius of the cylinders do not match, then it is treated as a cone.

If a wire contains only arcs, we can define a sphere whose center lies at the center of an arc, and check for consistency with the rest of the arcs. If a sphere is not an appropriate fit, we define a torus with the major radius set to the average of the two largest arcs and minor radius set to that of the smallest arc.

Faces. With wires and surfaces available, it is straightforward to combine them to build a face using the solid modeling kernel. Finally, to topologically connect the individual faces with each other, we sew the faces into shells, and further attempt to stitch the shells into a single solid model.

C HUMAN EVALUATION

As discussed in subsection 5.4, to evaluate the realism of the models generated by SolidGen, we perform a perceptual study using human evaluators recruited through Amazon’s Mechanical Turk service [22]. The crowd workers were shown pairs of images, one of which was generated by SolidGen or DeepCAD and the other randomly selected from the training set. The position of the image of the generated model was randomized to be at the top or the bottom of the pair. An example of an image pair is shown in Figure A2a. The crowd workers were asked to select the model which they found to be most “realistic”. To assist with this task we provided four examples of realistic models (Figure A2b) and “unrealistic” models (Figure A2c). The realistic examples were carefully chosen from the training set to include desirable properties like symmetry and clear design intent and function. For the unrealistic examples we deliberately selected models which had obvious problems like missing faces or which formed an incoherent collection of shapes.

In total 4400 pairs of images were shown to the crowd workers, half from SolidGen and half from DeepCAD. Each pair was independently judged by 7 crowd workers and we record the number of raters who identified the generated model as more realistic than randomly selected model from the training set. This gives us a “realism” score from 0–7 for each image pair. The percentage of image pairs with each realism are shown in the histogram in Figure 4 of the main paper.

If the human raters were selecting randomly between the two images then we would expect Figure 4 to form a binomial distribution. We see that for SolidGen the distribution is centered on a realism score of 3.5, but has wider tails than would be expected from chance alone. This indicates that while the realism of the models generated by SolidGen is very similar to the training data, the raters do tend to agree on the realism of individual examples to a greater extent than would be expected by chance alone.

For the DeepCAD data there is a clear skew towards the raters identifying the training set as more realistic.

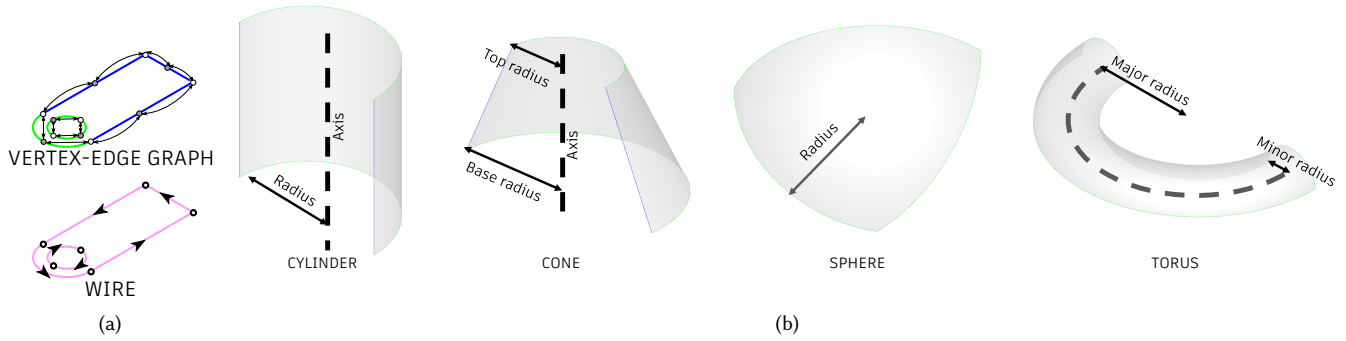


Fig. A1. (a) Vertex-edge graph used to build and orient the wires by finding cycles. (b) Identifying different kinds of surfaces from the curves (lines in blue, arcs in green) in the outer wire.

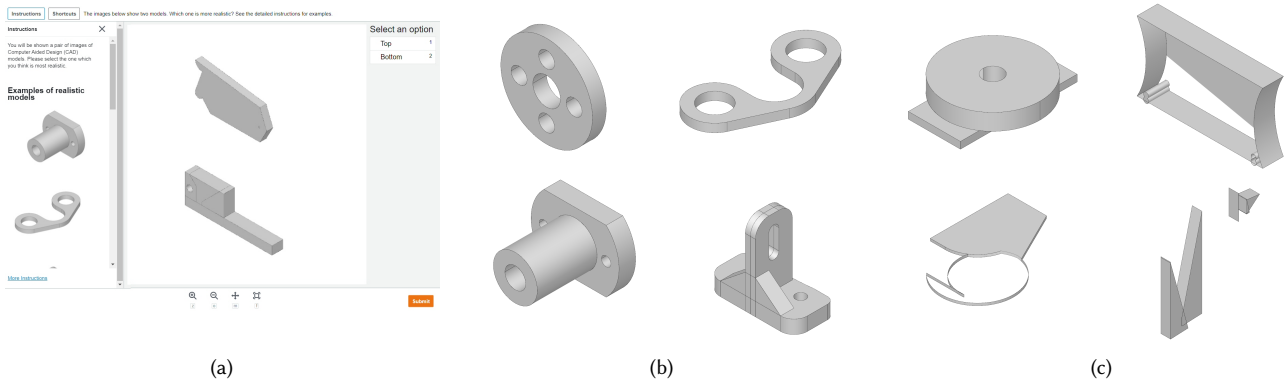


Fig. A2. (a) An example of an image pair shown to the crowd workers. (b) Examples of “realistic” models (from the DeepCAD training set) shown to the crowd workers. (c) Examples of unrealistic models. Two of these were generated by DeepCAD and two by SolidGen.

D GENERATION OF THE PARAMETRIC VARIATION DATASET

The parametric variation (PVar) dataset was created using constrained parametric sketches from the SketchGraphs dataset [28]. Geometry and constraints were first extracted from 60 hand picked sketches and additional constraints and parameters controlling the lengths of lines and radii of arcs and circles added one by one until the sketches were optimally constrained [6]. These parameters could then be varied to generate multiple sketch geometries, while the constraints enforce aspects of the design intent such as horizontal, vertical and parallel lines and concentric arcs and circles.

In cases where the sketch geometry defined multiple adjacent regions (see Figure A3 (a)), the curves were organized into a set of nested wires. The outermost wire is chosen to contain the union of the regions and inner wires chosen at random to avoid any two wires sharing the same curve. The outermost wire is first extruded by a random distance forming a base extrusion. The inner wires are then extruded, starting from the top plane of the base extrusion and a Boolean union or subtraction used to either add or remove material from the result. Figure A3 show the results of this process. Figure A4 shows one representative example from each class.

E ADDITIONAL RESULTS

We include additional results comparing DeepCAD [44] and SolidGen on the unconditional generation task in Figure A5 and Figure A6.

We show additional results for class-conditional generation on the PVar dataset in Figure A7.

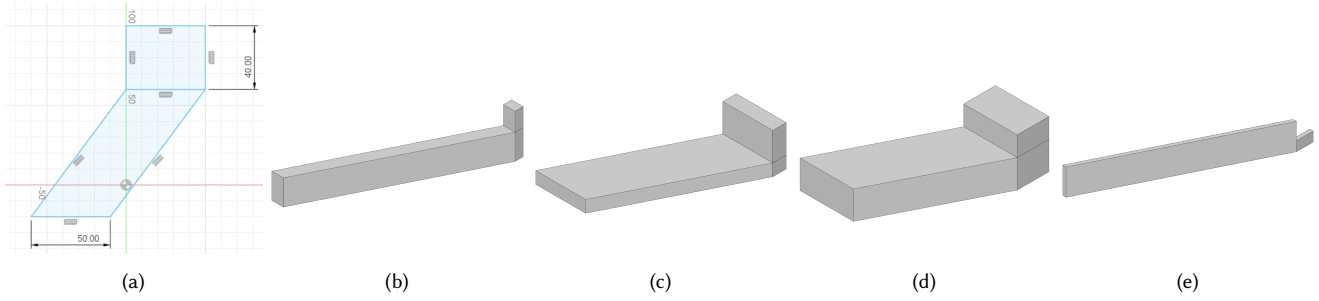


Fig. A3. (a) An example of one of the parametric sketch templates used to build the dataset. (b–d) Examples of generated models with the extrusion from the inner wire added to the base extrusion. Here we see the effect of modifying the parameters controlling both the sketch geometry and the lengths of the two extrusions. (e) The result of a Boolean subtraction of the inner wire.

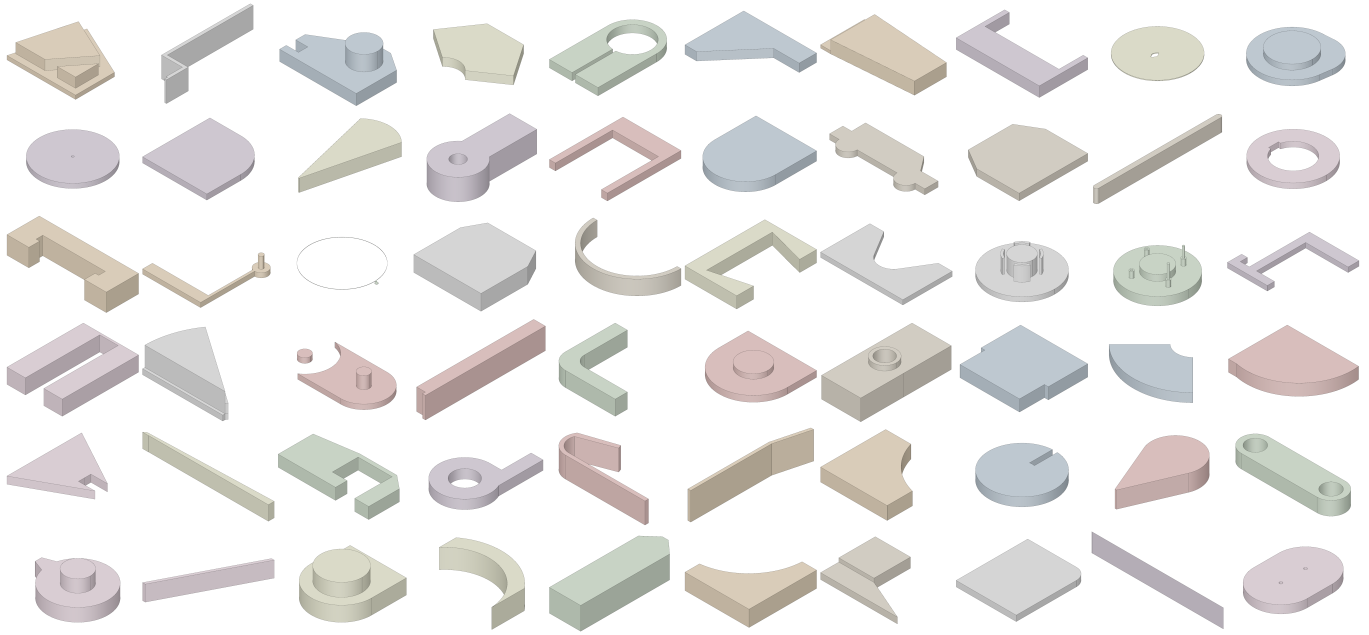
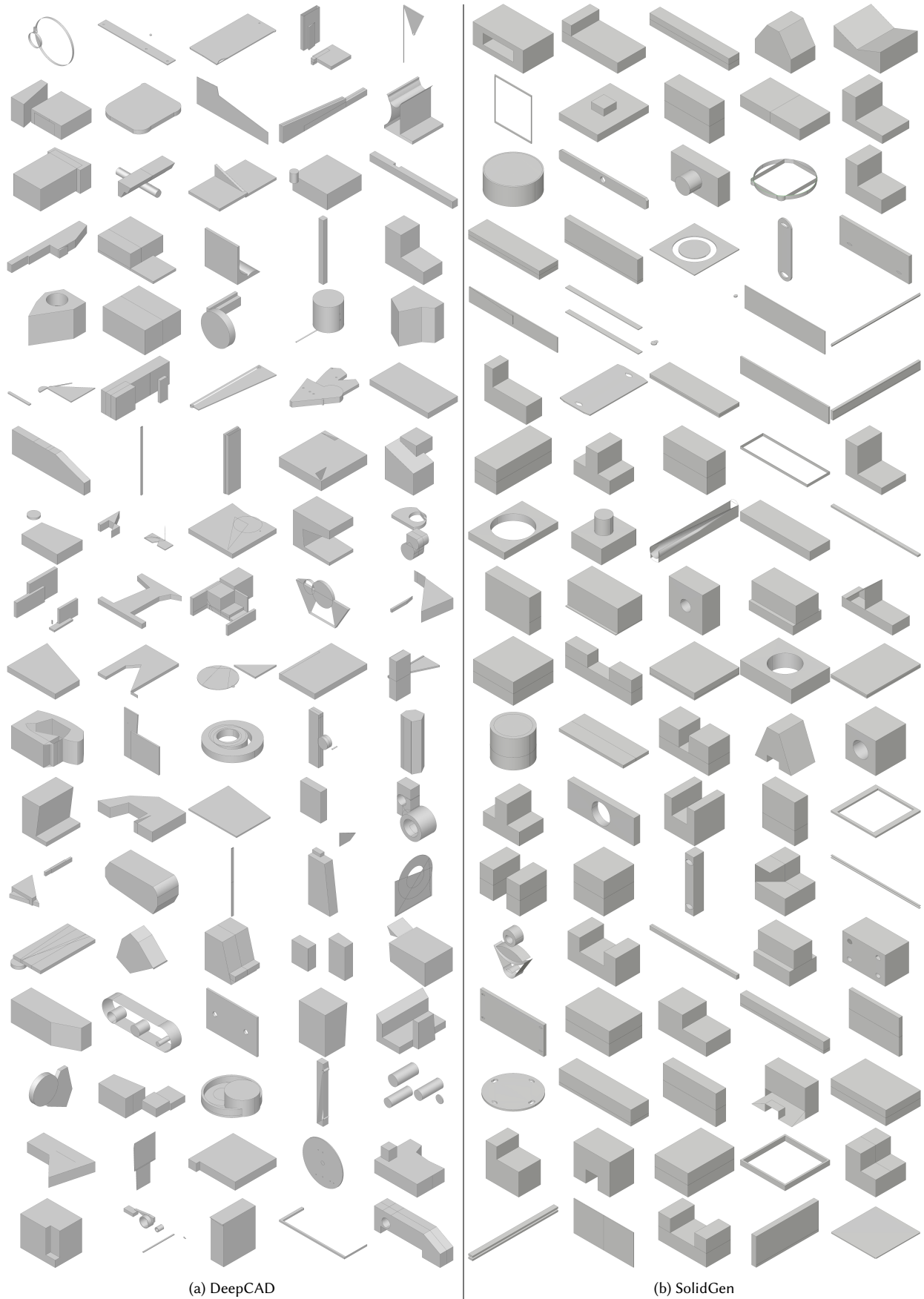


Fig. A4. Examples from each class in the PVar dataset.



(a) DeepCAD

(b) SolidGen

Fig. A5. Additional unconditional generation results.

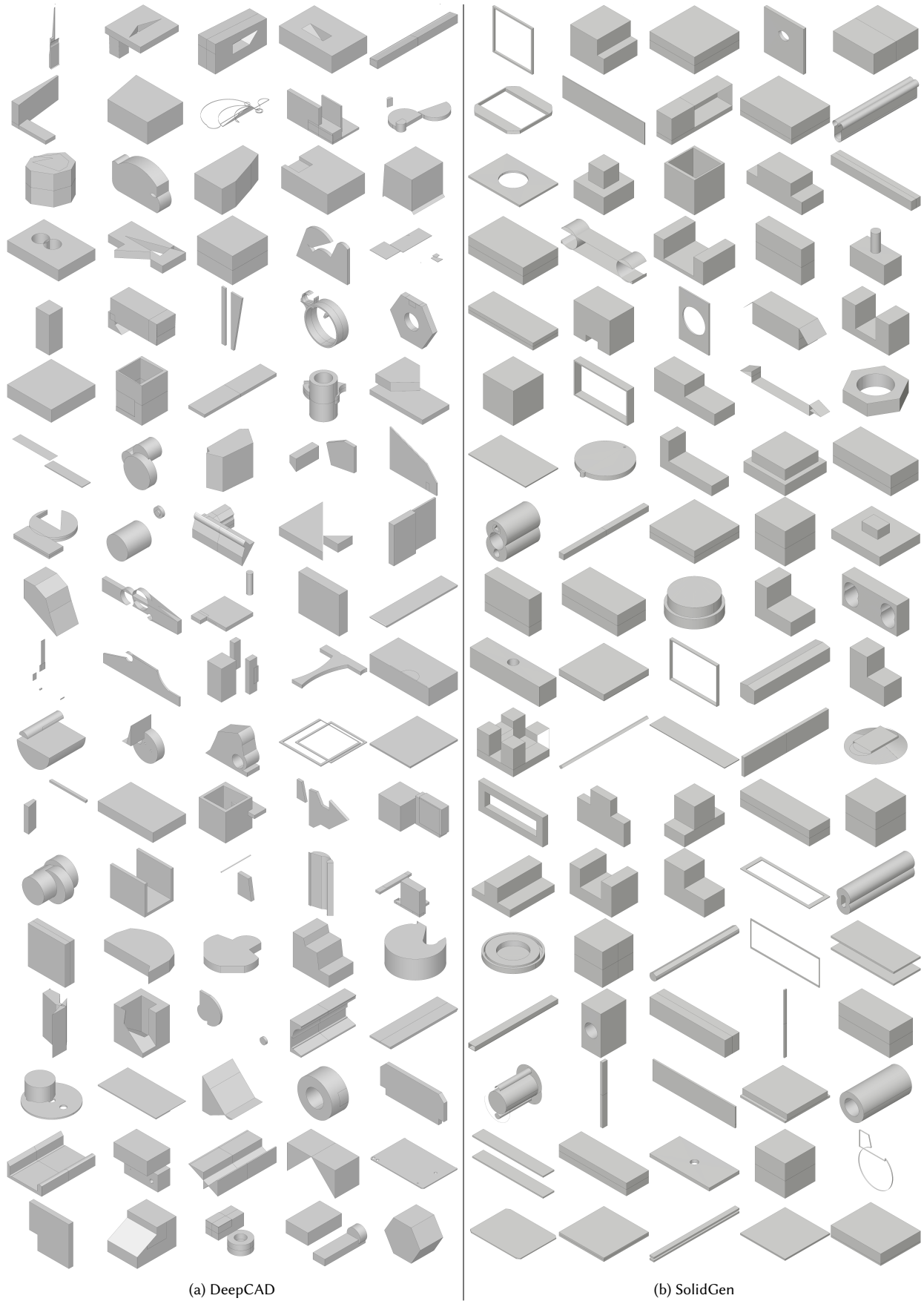


Fig. A6. Additional unconditional generation results.

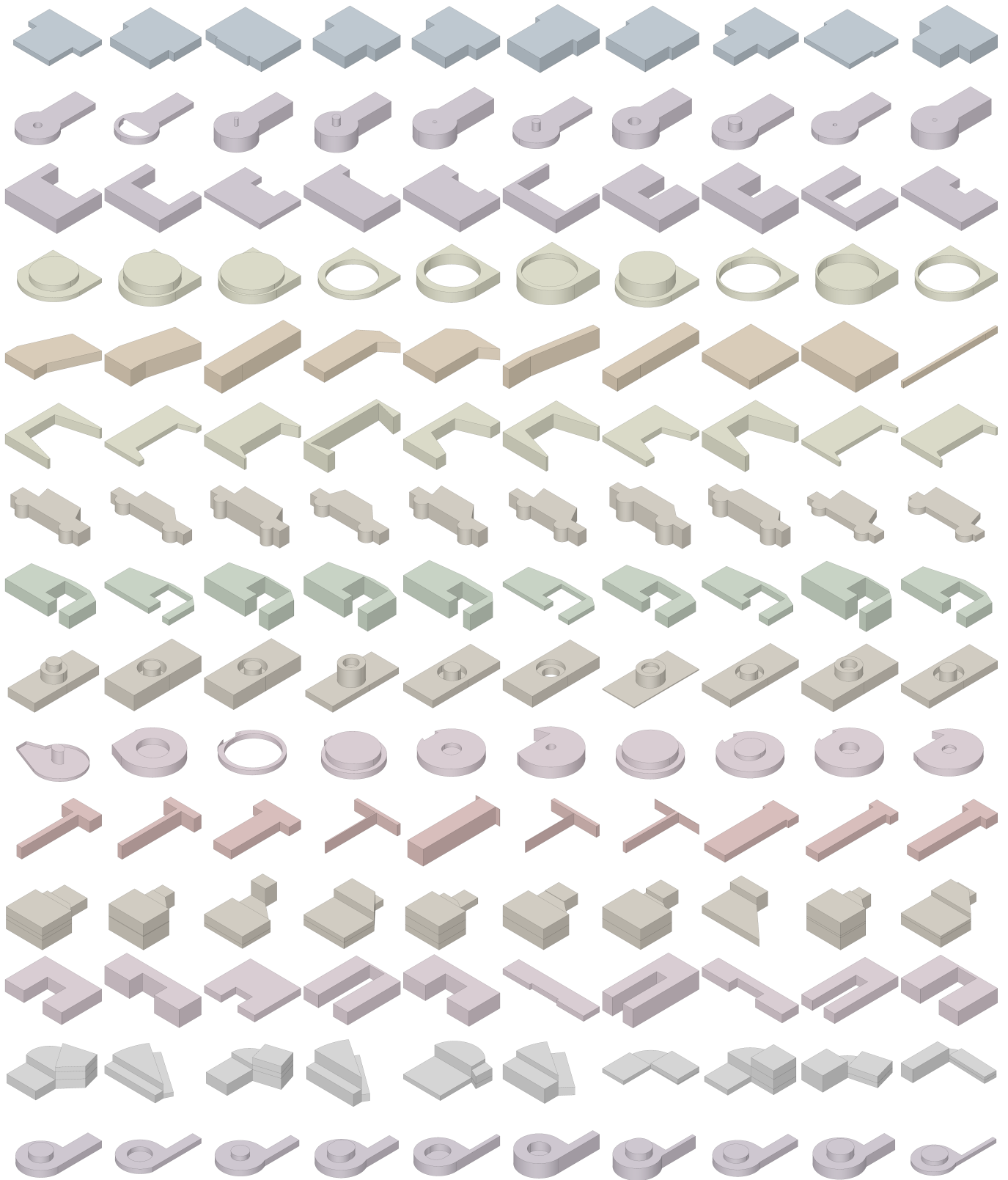


Fig. A7. Additional class-conditional generation results. Each row shows samples generated from the same class.